SolarPACES 2024, 30th International Conference on Concentrating Solar Power, Thermal, and Chemical Energy Systems

Receivers and Heat Transfer Media and Transport: Point Focus Systems

https://doi.org/10.52825/solarpaces.v3i.2305

© Authors. This work is licensed under a Creative Commons Attribution 4.0 International License

Published: 20 Nov. 2025

CFD Investigation of Particle Temperature in Fluidised Bed Solar Receivers

Mustafa Alqudah^{1,*} (D), Timothy Anderson² (D), and Alan Brent¹ (D)

¹Te Herenga Waka Victoria University of Wellington, Wellington 6012, Aotearoa New Zealand ²Charles Sturt University, Australia

*Correspondence: Mustafa Alqudah, mustafa.alqudah@vuw.ac.nz

Abstract. This study investigates the influence of fluidised bed solar receiver geometries and fluidisation velocity on particle temperature distribution and bed performance, with a focus on evaluating the feasibility of using a square shape for fluidised bed solar receivers. The research compares cylindrical and square bed geometries under varying fluidisation velocities to assess their impact on temperature profiles, and overall receiver performance. The results indicate that increasing fluidisation velocity enhances particle mixing and raises mean particle temperatures across both geometries, with the cylindrical bed showing higher mean temperatures at higher velocity. However, the square bed maintains better temperature uniformity, especially at higher velocity, which is advantageous for minimising hot spots and ensuring stable operation. While increased velocities improve bed dynamics and facilitate rapid collection of intermittent solar power, they also require higher pumping power and can lead to greater heat loss. Despite these benefits, further investigation is needed on the square shape, particularly in exploring uneven fluidisation regimes to reduce higher temperatures at the corners. Overall, the findings suggest that square-shaped fluidised beds offer a promising and feasible design alternative for solar receivers, balancing temperature uniformity and operational efficiency.

Keywords: Beam-Down Configuration, Computational Fluid Dynamics, Concentrated Solar Power, Fluidised Bed Solar Receiver, Minimum Fluidisation Velocity

1. Introduction

Concentrated Solar Power (CSP) systems are a promising renewable technology that harness and focus solar energy to produce high temperatures for electricity generation or chemical processes. Among various CSP configurations, the Beam-Down system stands out for redirecting concentrated sunlight from a central tower to a receiver at ground level. This setup allows more flexible receiver designs and is key to improving CSP efficiency.

Fluidised bed solar receivers are well-suited to Beam-Down systems due to their ability to handle high solar flux, achieving bed temperatures exceeding 1000 °C [1]. These receivers utilise a bed of fluidised particles to absorb and store solar energy, which is then transferred to a working fluid for power generation [2]. Bed particle temperature distribution significantly affects heat transfer and energy conversion. Uniform temperature is vital for system efficiency, while avoiding hot spots prevents material degradation and performance loss [3].

Fluidisation velocity strongly influences temperature uniformity, as it governs particle movement. Increased velocity improves circulation and reduces temperature gradients [4]. For instance, increasing velocity from 1.5 to 2.5 times the minimum fluidisation velocity ($U_{\it mf}$) reduced

peak bed temperature from 454 K to 384 K and raised average temperature from 315.9 K to 327.5 K [5]. Similar trends were observed at 3.0 and 4.0 U_{mf} [6].

Bed geometry also plays a crucial role in thermal behaviour and particle mixing. While cylindrical beds encourage faster mixing due to fewer dead zones, square and rectangular geometries offer practical advantages such as easier fabrication, larger size accommodation, and modular expansion [7,8,9]. Studies show that although cylindrical beds tend to reach higher average temperatures, square beds exhibit higher peaks and more localised hot spots [10], making them suitable for specific applications.

That said, although previous studies have explored the impact of fluidisation velocity on temperature distribution, the role of bed geometry still warrants further study. Research on fluidised bed receivers that integrates both factors is still in its early stages. This study addresses this gap by using Computational Fluid Dynamics (CFD) simulations to investigate how varying fluidisation velocities affect temperature distribution in both cylindrical and square fluidised bed geometries, with a focus on assessing the feasibility of square designs for future fluidised bed solar receivers. By evaluating the combined effects of these parameters, this research aims to enhance understanding and contribute to the development of more efficient and optimised fluidised bed receiver designs.

2. Numerical Model

2.1 Modelling of gas-solid flow

In this study a multiphase Eulerian-Eulerian (EE) approach was employed to simulate the gassolid flow in the Ansys-Fluent software package. In this approach the Navier-Stokes equations are used to describe each phase's behaviour.

The continuity equations for the fluid and solid phase are shown in equations (1) and (2) [11] [12]:

$$\frac{\partial}{\partial t} (\alpha_f \rho_f) + \nabla \cdot (\alpha_f \rho_f \vec{v}_f) = 0 \tag{1}$$

$$\frac{\partial}{\partial t} (\alpha_p \rho_p) + \nabla \cdot (\alpha_p \rho_p \vec{v}_p) = 0$$
 (2)

Similarly, the momentum balance equations for fluid and solid phases are shown in equations (3) and (4) [11] [12]:

$$\frac{\partial}{\partial t} (\alpha_f \rho_f \vec{v}_f) + \nabla \cdot (\alpha_f \rho_f \vec{v}_f \tau_f) = -\alpha_f \nabla p + \nabla \cdot \tau_f + \alpha_f \rho_f \vec{g} + K_{pf} (\vec{v}_p - \vec{v}_f)$$
 (3)

$$\frac{\partial}{\partial t} (\alpha_p \rho_p \vec{v}_p) + \nabla \cdot (\alpha_p \rho_p \vec{v}_p \tau_p) = -\alpha_p \nabla p + \nabla \cdot \tau_p + \alpha_p \rho_p \vec{g} + K_{fp} (\vec{v}_f - \vec{v}_p)$$
(4)

Where α_f and α_p are volume fractions of the gas and particles, ρ_f and ρ_p are the densities of the gas and particles, \vec{v}_f and \vec{v}_p are the gas and solid phase velocities, p is the gas pressure shared by both the gas and solid phases, τ_f and τ_p represent the gas and solid phase stress tensors, g is the gravitational acceleration, and K_{fp} is the interphase momentum exchange coefficient between the gas and solid particles per unit cell volume.

2.2 Radiative heat transfer

The P1 radiation model was implemented to assess the radiation heat transfer to the bed. Thus, the transport equation for the incident radiation can be written as shown in equation [5] [13]:

$$\nabla \cdot (\Gamma \nabla G) + 4\pi (an^2 \frac{\sigma T^4}{\pi} + E_p) - (a + a_p)G = 0$$
 (5)

Where Γ is the radiation diffuse coefficient, G is the incident radiation, a is absorption coefficient of the fluid, n is the reflective index, σ is the Stefan–Boltzmann constant, E_p is the equivalent emission of the particles, a_p is the equivalent particle coefficient absorption coefficient.

Implementing the P1 model for the thermal wall radiative heat flux was summarised by Marshak [5] [14] and is described by equation (6):

$$-q_w = \Gamma_w \cdot \left(\frac{\partial G}{\partial n}\right)_w = \frac{\epsilon_w}{2(2-\epsilon_w)} \cdot (4\sigma T_w^4 - G_w) \tag{6}$$

3. Modelling Setup and Boundary Conditions

3.1 Receiver geometries

This study investigates particle temperature in two fluidised bed solar receiver geometries: cylindrical and square. Both designs share identical cross-sectional areas and volumes to enable fair comparison. The cylindrical bed dimensions match those reported in [5, 15], with a diameter of 76.2 mm and a height of 500 mm. The square bed maintains the same height and a side length of 67.5 mm to ensure equal area. Figure 1 presents both configurations.

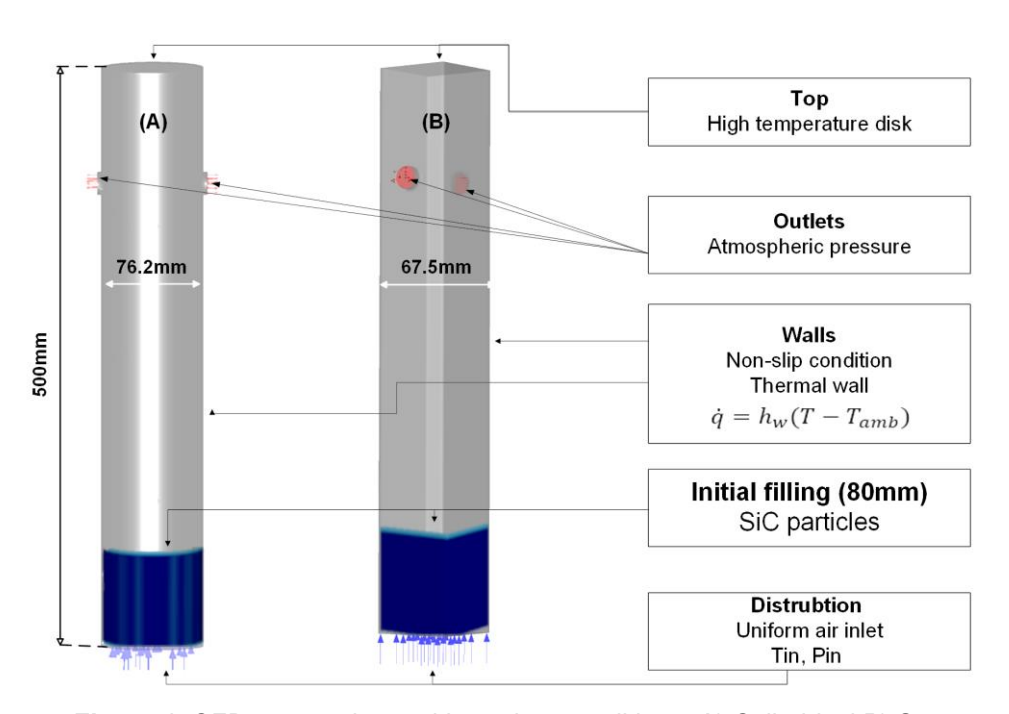


Figure 1. CFD geometries and boundary conditions, A) Cylindrical B) Square

Furthermore, Figure 1 illustrates the boundary conditions used in the simulation cases. At the inlet, air is uniformly distributed at a temperature of 298.15 K and exits the domain through two outlet ports at atmospheric pressure. All lateral walls are treated as thermal boundaries with no-slip conditions applied to both the gas and solid phases. Thermal losses through the receiver walls are modelled using a convective heat transfer boundary condition. The top surface of the receiver was modelled as a high-temperature wall maintained at 741.29 K, acting as a uniform radiation source for both geometries.

3.2 Fluidising velocity and particle properties

To investigate the impact of fluidisation velocity on particle temperature within fluidised bed solar receivers, two distinct velocities were simulated: a medium velocity (2 U_{mf}) and a high velocity (4 U_{mf}). These velocities correspond to twice and four times the U_{mf} measured in experiments with SiC particles (0.09 m/s, as reported in [15] and [16]). This selection allows for the evaluation of effects under typical operating conditions (2 U_{mf}) as well as significantly higher regimes (4 U_{mf}) on bed behaviour. As illustrated in Figure 2, higher velocities can shift the bed between different fluidisation regimes [17], which will inevitably influence the particle temperature, noting that the bubbling regime is currently preferred for solar receivers.

It is anticipated that these varying fluidisation velocities, which alter the fluidisation behaviour, will significantly impact particle temperature distribution within the receiver. This study builds on previous research, which typically focused on velocities up to 2.5 U_{mf}, by examining a broader range of velocities and their potential effects on the performance of solar receivers.

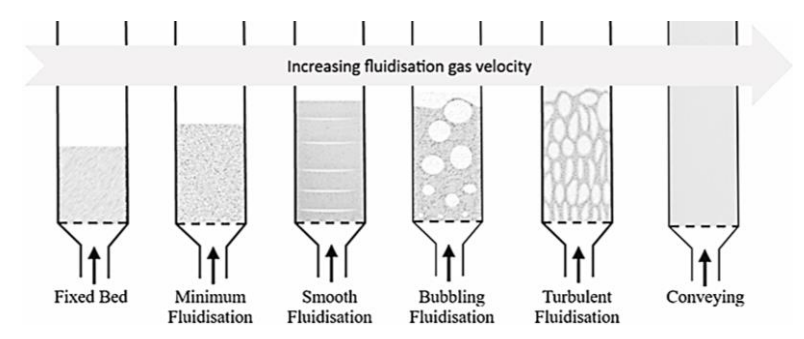


Figure 2. Gas velocity relation with fluidisation regime.

This study uses silicon carbide (SiC) as the particle material for the fluidised beds, as supported by [18] [19] and [15]. These studies compared various materials, including sand, silicon, and carbon, focusing on thermal and optical properties, mechanical resistance, storage efficiency, and absorptivity. They concluded that SiC is superior due to its high absorptivity, excellent thermal and optical properties, and strong mechanical resistance. The properties of SiC used in this study are as follows: the density is 3220 kg/m³, the mean particle diameter is 406.2 µm, and the specific heat capacity is 1.27 kJ/kg·K [14].

3.3 Radiation boundary condition

The radiation boundary condition in this study was defined based on the experimental work of Díaz-Heras et al. [15], where a 2 kW Xenon lamp simulated a beam-down CSP configuration. This setup produced a mean radiation flux of 140.63 W and a peak flux of 65 kW/m² on the bed surface. To replicate these conditions in the numerical model, a high-temperature ceiling was applied as the radiation source. Following the approach in [5], a fixed top wall temperature of 741.29 K was used, corresponding to the mean radiation flux measured experimentally. This uniform temperature distribution, as illustrated in Figure 1, was implemented for both cylindrical and square receiver geometries to ensure consistent irradiation conditions across the bed surface.

3.4 Numerical implementation

In performing the simulations, an initial fixed bed height of 80 mm was used, with a particle volume fraction set at 0.50. The gas-particle heat transfer coefficient was determined using the model of Gunn et al. [20], while the gas-particle drag coefficient was based on the model of Wen and Yu [21]. The restitution coefficient was set at 0.9.

The phase-coupled SIMPLE scheme was used to manage the coupling between pressure and momentum. Spatial discretization of the gradient was performed using the least squares cell-based method, while second-order discretization was applied to the pressure. The energy and momentum equations were discretized using a first-order unwinding scheme. The governing equations were solved using Ansys Fluent v2024R1, with under-relaxation factors set at 0.3 for pressure, 0.7 for momentum, 0.5 for volume fraction, and 1.0 for both energy and P1. The CFD time step was consistently maintained at 10e-3 seconds across all cases.

4. Results and Discussion

The numerical model was validated through a comparison with experimental data, focusing on a cylindrical fluidised bed operating at 2 U_{mf} with a uniform fluidising air pattern and 180 seconds of irradiation. The methodology employed in this study closely aligns with the approach validated by [10], ensuring consistency and reliability. Transient simulations were conducted for 180 seconds using a commercial CFD solver, providing a robust basis for the subsequent analysis.

4.1 Effect of geometry

To evaluate the impact of bed geometry on particle temperature distribution, Figure 3 presents the relationship between particle temperature and particle volume fractions at a fluidisation velocity of 2 U_{mf} . The results indicate that both geometries exhibit similar performance, with a slight advantage observed for the cylindrical shape. The particle temperature remains relatively uniform at higher volume fractions, as reflected by the flattening of the curve. However, at lower volume fractions, the temperature distribution becomes less uniform, with some particles reaching significantly higher temperatures compared to the average bed temperature. This phenomenon is likely due to particle cloud formation or material splashing when air bubbles erupt.

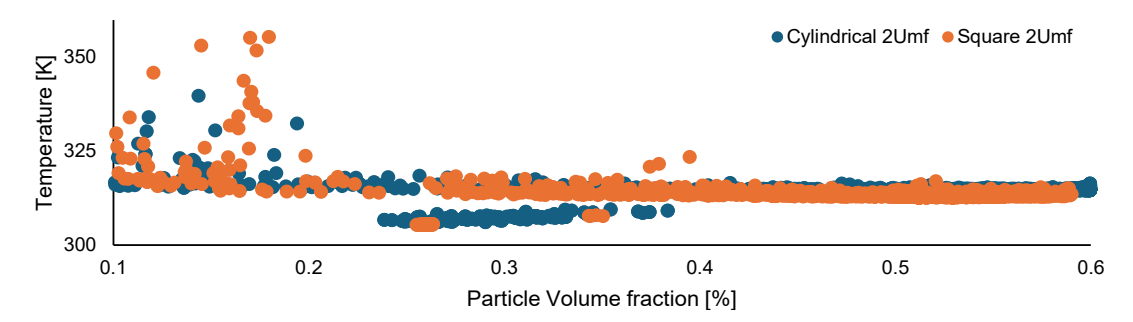


Figure 3. Particle temperature vs volume fraction at 2 U_{mf}

Another notable result is the temperature distribution within the bed, which illustrates how temperature varies across different particle positions. Figure 4 presents temperature contours at a 6 mm bed height, revealing that the highest temperatures occur near the walls in both geometries. The cylindrical bed (Figure 4-A) demonstrates slightly less temperature variation compared to the square bed. In contrast, the square geometry (Figure 4-B) shows higher temperatures around the corners, likely due to less fluidisation and mixing in those regions.

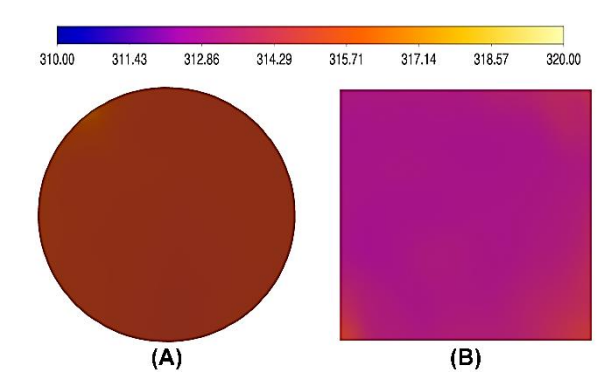


Figure 4. Particle temperature contours at 6 mm bed height

4.2 Effect of fluidizing velocity

Increasing fluidization velocity enhances mixing and particle circulation, which directly influences particle temperature. Figure 5 illustrates this effect by showing particle temperature distribution across the volume fraction for both geometries at 4 U_{mf} . It is evident that particle temperatures rise with increased velocity compared to Figure 3. Interestingly, in the 2 U_{mf} model, the cylindrical bed exhibits higher temperatures at 4 U_{mf} . Additionally, a significant number of particles show higher temperatures along the flat curve, particularly at high volume fractions, increasing the risk of hot spots that could compromise receiver operation and cause material degradation. The square bed demonstrates more uniform particle temperatures, though both geometries experience uneven temperatures at low volume fractions, which raises the risk of overheating. However, in the square bed at 4 U_{mf} , this issue improves with fewer particles observed.

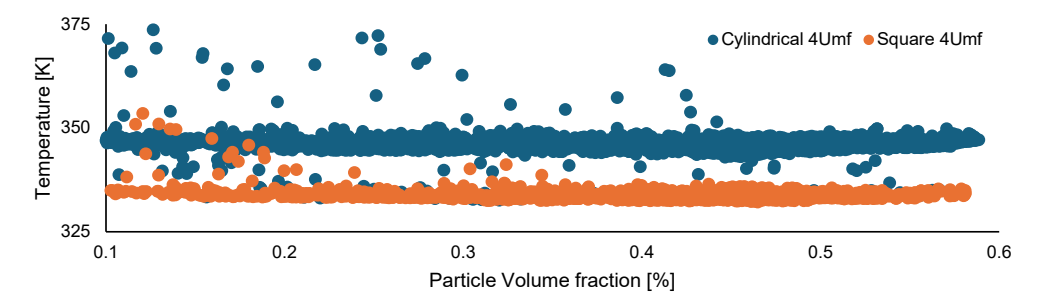


Figure 5. Particle temperature vs volume fraction at 4 U_{mf}

Moreover, Figure 6 shows that increasing the fluidization velocity from 2 to 4 U_{mf} elevates the overall mean particle temperature in both geometries, with the cylindrical bed maintaining a higher mean temperature. Additionally, the peak particle temperature decreases in both geometries as velocity increases. These two indicators suggest that bed performance improves with higher fluidization velocity.

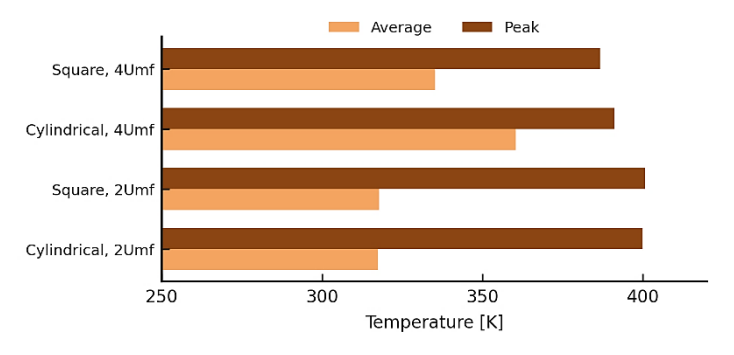


Figure 6. Particles temperature for different fluidization gas velocity

5. Conclusion

This study explored the effects of fluidised bed solar receiver geometries and fluidisation velocity on particle temperature. The key findings are:

- Increasing fluidisation velocity enhances bed dynamics and particle mixing, leading to higher particle temperatures.
- At lower velocities, cylindrical and square beds exhibit similar behaviour. However, at higher velocities, the cylindrical bed achieves a higher mean temperature, while the square bed maintains better temperature uniformity.
- Higher velocities, while beneficial for more rapid collection of fluctuating solar power, require greater pumping power and may result in increased heat loss.
- The results suggest that square-shaped beds are a viable option for fluidised bed receivers, though further investigation is needed to explore uneven fluidisation regimes to reduce high temperatures at the corners.

Data availability statement

This study is part of a PhD thesis, and the data will be available upon graduation.

Author contributions

M. Alqudah: methodology, built the simulation, collected and analysed the data and writing. **T. Anderson**: supervision, writing, review and editing. **A. Brent**: supervision, writing, review and editing

Competing interests

The authors declare that they have no competing interests.

References

- [1] J. V. Briongos, J. Gómez-Hernández, P. A. González-Gómez, and D. Serrano, "Two-phase heat transfer model of a beam-down gas-solid fluidized bed solar particle receiver," *Solar Energy*, vol. 171, pp. 740–750, Sep. 2018, doi: 10.1016/j.solener.2018.07.016.
- [2] S. Bellan, N. Gokon, K. Matsubara, H. S. Cho, and T. Kodama, "Heat transfer analysis of 5kWth circulating fluidized bed reactor for solar gasification using concentrated Xe light radiation," *Energy*, vol. 160, pp. 245–256, Oct. 2018, doi: 10.1016/j.energy.2018.06.212.
- [3] P. Salatino, P. Ammendola, P. Bareschino, R. Chirone, and R. Solimene, "Improving the thermal performance of fluidized beds for concentrated solar power and thermal energy storage," *Powder Technology*, vol. 290, pp. 97–101, Mar. 2016, doi: 10.1016/j.pow-tec.2015.07.036.
- [4] X. Li *et al.*, "Experimental and numerical study on thermal performance of an indirectly irradiated solar reactor with a clapboard-type internally circulating fluidized bed," *Applied Energy*, vol. 305, p. 117976, Jan. 2022, doi: 10.1016/j.apenergy.2021.117976.
- [5] M. Díaz-Heras, J. I. Córcoles, J. F. Belmonte, and J. A. Almendros-Ibáñez, "3D numerical simulation of a directly irradiated bubbling fluidized bed with SiC particles," *Applied Thermal Engineering*, vol. 190, p. 116812, May 2021, doi: 10.1016/j.ap-plthermaleng.2021.116812.
- [6] M. Alqudah, T. Anderson, and R. Nates, "The effect of fluidizing gas velocity on a fluidized bed solar receiver," in 2022 Asia Pacific Solar Research Conference: APSRC 2022, 2022.

- Accessed: Jul. 26, 2024. [Online]. Available: https://apvi.org.au/solar-research-conference/wp-content/uploads/2023/02/Anderson-The-effect-of-fluidizing-gas-velocity-on-a-fluidized-bed-solar-receiver.pdf
- [7] S. Gorji-Kandi, S. M. Alavi-Amleshi, and N. Mostoufi, "Experimental investigating the effect of bed geometry on solids mixing in fluidized beds," *Particulate Science and Technology*, vol. 34, no. 2, pp. 127–133, Mar. 2016, doi: 10.1080/02726351.2015.1054532.
- [8] E. H. van der Meer, R. B. Thorpe, and J. F. Davidson, "Flow patterns in the square cross-section riser of a circulating fluidised bed and the effect of riser exit design," *Chemical Engineering Science*, vol. 55, no. 19, pp. 4079–4099, Oct. 2000, doi: 10.1016/S0009-2509(00)00081-6.
- [9] Z. Wang, S. Sun, H. Chen, Q. Deng, G. Zhao, and S. Wu, "Experimental investigation on flow asymmetry in solid entrance region of a square circulating fluidized bed," *Particuology*, vol. 7, no. 6, pp. 483–490, Dec. 2009, doi: 10.1016/j.partic.2009.07.004.
- [10]M. Alqudah, T. Anderson, and J. Hinkley, "A comparison of fluidised bed solar receiver geometries," in *2023 Asia-Pacific Solar Research Conference*, 2023. Accessed: Jul. 26, 2024. [Online]. Available: https://apvi.org.au/solar-research-conference/wp-content/up-loads/2023/12/Algudah-M-A-comparison-of-fluidised-bed-solar-receiver-geometries.pdf
- [11]M. Adnan, J. Sun, N. Ahmad, and J. J. Wei, "Comparative CFD modeling of a bubbling bed using a Eulerian–Eulerian two-fluid model (TFM) and a Eulerian-Lagrangian dense discrete phase model (DDPM)," *Powder Technology*, vol. 383, pp. 418–442, May 2021, doi: 10.1016/j.powtec.2021.01.063.
- [12] "ANSYS FLUENT 12.0 Theory Guide 16.5 Eulerian Model Theory." Accessed: Apr. 28, 2024. [Online]. Available: https://www.afs.enea.it/project/neptunius/docs/fluent/html/th/node319.htm
- [13] "ANSYS FLUENT 12.0 Theory Guide 5.3.3 P-1 Radiation Model Theory." Accessed: Apr. 29, 2024. [Online]. Available: https://www.afs.enea.it/project/neptunius/docs/fluent/html/th/node112.htm
- [14]R. E. Marshak, "Note on the Spherical Harmonic Method As Applied to the Milne Problem for a Sphere," *Phys. Rev.*, vol. 71, no. 7, pp. 443–446, Apr. 1947, doi: 10.1103/PhysRev.71.443.
- [15]M. Díaz-Heras, C. Barreneche, J. F. Belmonte, A. Calderón, A. I. Fernández, and J. A. Almendros-Ibáñez, "Experimental study of different materials in fluidized beds with a beam-down solar reflector for CSP applications," *Solar Energy*, vol. 211, pp. 683–699, Nov. 2020, doi: 10.1016/j.solener.2020.07.011.
- [16]M. Díaz-Heras, J. D. Moya, J. F. Belmonte, J. I. Córcoles-Tendero, A. E. Molina, and J. A. Almendros-Ibáñez, "CSP on fluidized particles with a beam-down reflector: Comparative study of different fluidization technologies," *Solar Energy*, vol. 200, pp. 76–88, Apr. 2020, doi: 10.1016/j.solener.2019.09.006.
- [17] R. Cocco, S. B. R. Karri, and T. Knowlton, "Introduction to Fluidization," *Back to Basics*, p. 9, 2014.
- [18]C. Tregambi *et al.*, "Experimental characterization of granular materials for directly irradiated fluidized bed solar receivers," presented at the SOLARPACES 2018: International Conference on Concentrating Solar Power and Chemical Energy Systems, Casablanca, Morocco, 2019, p. 030060. doi: 10.1063/1.5117572.
- [19]M. Díaz-Heras, A. Calderón, M. Navarro, J. A. Almendros-Ibáñez, A. I. Fernández, and C. Barreneche, "Characterization and testing of solid particles to be used in CSP plants: Aging and fluidization tests," *Solar Energy Materials and Solar Cells*, vol. 219, p. 110793, Jan. 2021, doi: 10.1016/j.solmat.2020.110793.
- [20] D. J. Gunn, "Transfer of heat or mass to particles in fixed and fluidised beds," *International Journal of Heat and Mass Transfer*, vol. 21, no. 4, pp. 467–476, Apr. 1978, doi: 10.1016/0017-9310(78)90080-7.
- [21] C. Y. Wen, "Mechanics of fluidization," *The Chemical Engineering Progress Symposium Series*, vol. 62, 1966, pp. 100–111.